ADVANCED FUNCTIONAL MATERIALS
www.afm-journal.de

Homogeneous and Fast Ion Conduction of PEO-Based Solid-State Electrolyte at Low Temperature

Shengjun Xu, Zhenhua Sun, Chengguo Sun, Fan Li, Ke Chen, Zhihao Zhang, Guangjin Hou, Hui-Ming Cheng, and Feng Li**

Poly(ethylene oxide) (PEO)-based electrolytes are promising for all-solid-state batteries but can only be used above room temperature due to the high-degree crystallization of PEO and the intimate affinity between ethylene oxide (EO) chains and lithium ions. Here, a homogeneous-inspired design of PEO-based solid-state electrolytes with fast ion conduction is proposed. The homogeneous PEO-based solid-state electrolyte with an adjusted succinonitrile (SN) and PEO molar ratio simultaneously suppresses the PEO crystallization and mitigates the affinity between EO and Li^+. By adjusting the molar ratio of SN to PEO (SN:EO ≈ 1:4), channels providing fast Li^+ transport are formed within the homogeneous solid-state polymer electrolyte, which increases the ionic conductivity by 100 times and enables their application at a low temperature (0–25 °C), together with the uniform lithium deposition. This modified PEO-based electrolyte also enables a $LiFePO_4$ cathode to achieve a superior Coulombic efficiency (>99%) and have a long life (>750 cycles) at room temperature. Moreover, even at a low temperature of 0 °C, 82% of its room-temperature capacity remains, demonstrating the great potential of this electrolyte for practical solid-state lithium battery applications.

1. Introduction

Batteries that are composed of lithium metal anodes, all-solid-state electrolytes and high-energy cathode materials have been considered as a promising electrochemical energy storage system to meet the ever-increasing requirements of safe power supply techniques.[1,2] Among many all-solid-state electrolytes, the poly(ethylene oxide) (PEO)-based system shows significant advantages, such as easy fabrication, good mechanical flexibility, low interface resistance and good stability with lithium metal.[3,4] However, a critical problem of the PEO-based all-solid-state electrolytes is their low ionic conductivity (10^{-8}–10^{-7} S cm^{-1}) at room temperature, which is caused by limited chain motion and thus results in high optimal operating temperatures of around 50–70 °C.[5,6] To improve the ionic conductivity, various approaches have been developed,[7–11] among which adding fillers has been demonstrated to be a simple way of suppressing PEO crystallization and promoting the motion of ethylene oxide (EO) chains.[12–17] Nevertheless, no composite PEO-based electrolytes have been able to meet the need for all-solid-state batteries operating at room temperature.[18,19] This is because the effect of adding fillers on Li^+ transport only works in a specified position, and cannot produce fast Li^+ transport channels within homogeneous solid-state polymer electrolytes.

The transport of lithium ions (Li^+) in PEO-based all-solid-state electrolytes is realized by complexation and decomplexation with oxygen in the PEO during charge and discharge.[20] The complexation modes of Li^+ in the intramolecular and intermolecular of PEO are shown in Figure S1a and S1b, Supporting Information. To form fast Li^+ transport channels in all-solid-state PEO-based electrolytes, the distance between Li^+ binding sites in the PEO and the chemical environment of

S. Xu, Prof. Z. Sun, Prof. C. Sun, K. Chen, Z. Zhang, Prof. H.-M. Cheng, F. Li
Shenyang National Laboratory for Materials Science
Institute of Metal Research
Chinese Academy of Science
Shenyang 110016, China
E-mail: cheng@imr.ac.cn; fli@imr.ac.cn

S. Xu, Prof. Z. Sun, Z. Zhang, Prof. F. Li
School of Materials Science and Engineering
University of Science and Technology of China
Shenyang 110016, China

The ORCID identification number(s) for the author(s) of this article can be found under https://doi.org/10.1002/adfm.202007172.

DOI: 10.1002/adfm.202007172

F. Li, Prof. G. Hou
State Key Laboratory of Catalysis
Dalian Institute of Chemical Physics
Chinese Academy of Science
Dalian 116023, China

F. Li
University of Chinese Academy of Sciences
Beijing 100039, China

K. Chen
School of Physical Science and Technology
ShanghaiTech University
Shanghai 201210, China

Prof. H.-M. Cheng
Shenzhen Geim Graphene Center
Tsinghua-Berkeley Shenzhen Institute
Tsinghua University
Shenzhen 518055, China

the Li^+ must be considered.[19] The distance between adjacent Li^+ binding sites (two adjacent oxygens) in a PEO molecule is the chain length of $-O-CH_2-CH_2-O-$ and Li^+ transported gradually with the length of $-O-CH_2-CH_2-O-$ in the intramolecular and intermolecular.[21–23] (Figure S1c and S1d, Supporting Information). Accordingly, this added filler should meet two requirements: (1) the size of the filler should be close to the chain length of $-O-CH_2-CH_2-O-$ and (2) the additive must effectively optimize the chemical environment of Li^+. For these reasons, the size mismatching of inorganic fillers (usually beyond 50 nm) with $-O-CH_2-CH_2-O-$ (near 0.5 nm) would lead to the rate-limiting step is always exited (Figure S1e, Supporting Information). But for solid-state organic materials that have a smaller molecular size (near 0.5 nm), the size matching of solid-state organic fillers with $-O-CH_2-CH_2-O-$ contributes to the formation of continuous Li^+ transport channels on the nanoscale as shown in Figure S1f, Supporting Information. As a result, it is better to choose a solid-state organic material with small molecule size as the filler rather than an inorganic particle. Uniform channels that allow fast Li^+ transport may be formed and Li^+ could move rapidly in PEO-based electrolytes modified by solid-state organic materials.

Succinonitrile (SN) is a solid-state organic material, in which Li^+ moves easily to give hopping conduction,[24,25] and has been used to improve the performance of PEO-based electrolytes.[26–30] In these studies, the effect of adding SN to a PEO-based electrolyte is generally to inhibit its crystallization and promote the solubility of lithium salts, so that it plays a role in the local ion conductivity of the solid-state electrolytes. However, the homogeneous and fast ion transport channels in solid-state electrolytes have not been formed across the entire system. Furthermore, the SN content was limited to 10 wt% because free-standing membranes failed to produce at higher content.[29,31,32] It was unfeasible to construct homogeneous and fast ion transport channels by further increasing the SN content. Typically, the addition of 10 wt% SN with a low SN/EO molar ratio (SN:EO ≈ 1:12) produces nonuniform channels and slow Li^+ transport in PEO-based solid-state electrolytes, therefore, more SN were required to form a mixed homogeneous phase with the "improved area" (homogeneous and fast Li^+ channels).

Here, we construct free-standing membranes with a high SN/EO molar ratio (SN:EO = 1:4) and form homogeneous and fast ion transport channels. These membranes (≈150 µm thick) were prepared by a solvent casting method and the key to the preparation process is reducing the Li^+ concentration (Li^+: EO) to 1:32. The formed homogeneous PEO-based solid-state electrolyte with fast Li^+ transport channels allows an ionic conductivity of 0.19 mS cm^{-1} at room temperature (25 °C). Benefiting from these Li^+ transport channels, the PEO-based electrolyte enabled a $LiFePO_4$ cathode to achieve a high capacity (145.5 mAh g^{-1} at 0.5C) and long-term cycling stability (≈750 cycles) at room temperature. Even at 0 °C, a Li‖$LiFePO_4$ cell showed a high discharge capacity of 118.6 mAh g^{-1} at 0.1C after 180 cycles.

2. Results and Discussion

The significance of a homogeneous PEO-based solid-state electrolyte with fast Li^+ transport channels is summarized in **Figure 1**. Figure 1a illustrates a typical PEO-based solid-state electrolyte (PEO32) without modification. It has a low ionic conductivity due to its high degree of crystallization and intimate affinity of ethylene oxide chains for Li^+. To form uniform, fast ion channels in the solid-state polymer electrolyte, SN was chosen as a

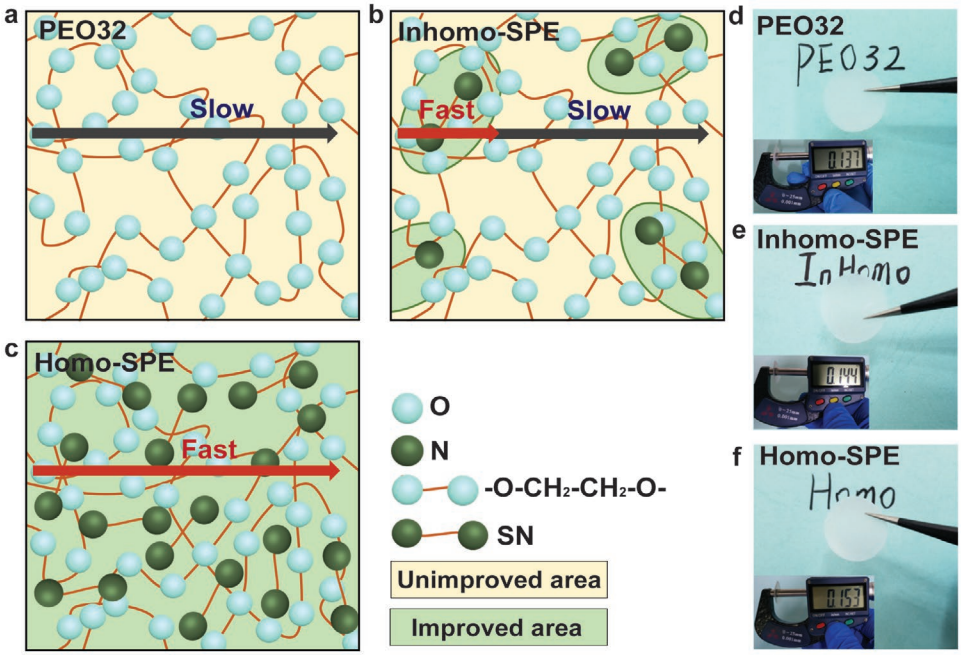

Figure 1. Schematic of PEO-based electrolytes. (a–c) Li^+ transport modes: a) PEO32, b) Inhomo-SPE, and c) Homo-SPE. (d–e) Optical photographs: d) PEO32, e) Inhomo-SPE and f) Homo-SPE.

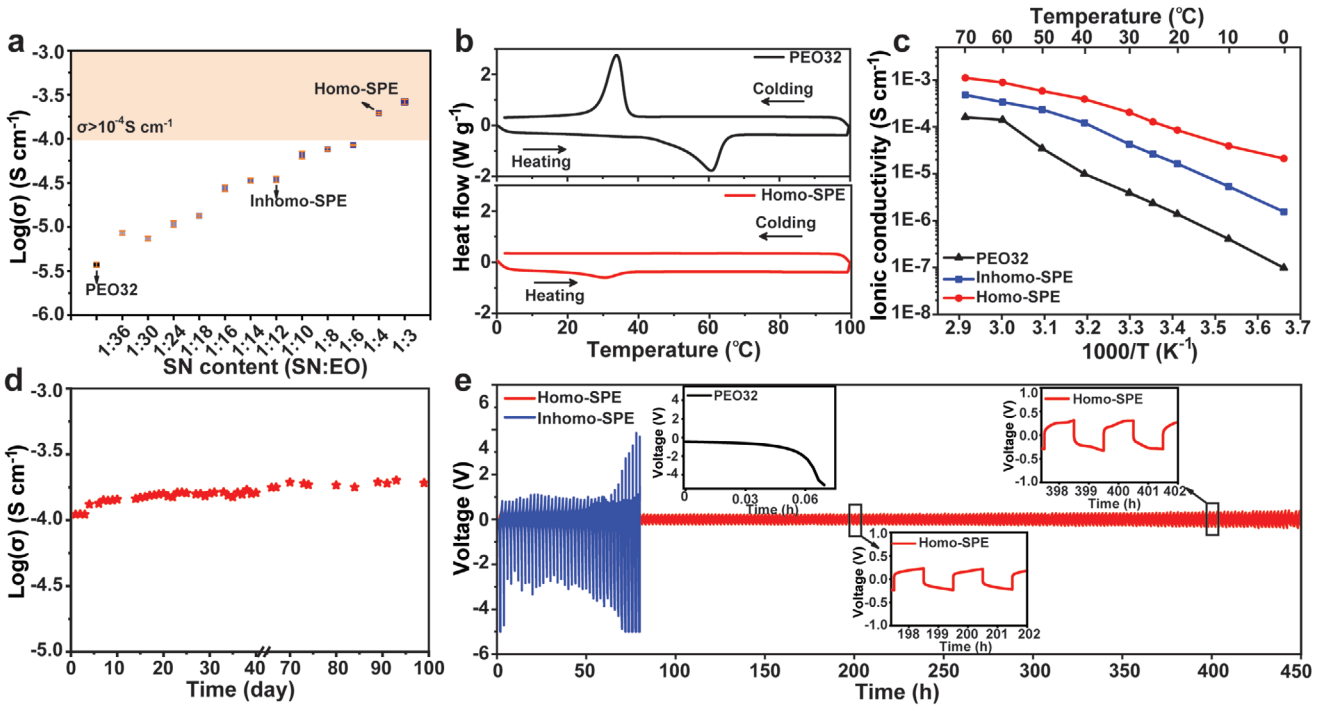

Figure 2. Physicochemical and electrochemical characterization of solid-state electrolytes. a) Variation of the ionic conductivity at room temperature of PEO-based solid-state electrolytes (Li^+:EO = 1:32) with different amounts of added SN. b) DSC profiles of PEO32 and Homo-SPE. c) Arrhenius plots of the ionic conductivity of various solid-state electrolytes. d) Stability of the ionic conductivity of Homo-SPE. e) Symmetric-cell cycling with Inhomo-SPE (blue line) and Homo-SPE (red line). The current density was fixed at 0.1 mA cm^{-2} (with areal capacity of 0.1 mAh cm^{-2}) during the tests. Insets: Symmetric-cell with PEO32 (black line), enlarged profiles at the two consecutive cycle numbers noted (red line).

filler because its molecular size (NC—CH_2—CH_2—CN) matches the distance of Li^+ binding sites in PEO (—O—CH_2—CH_2—O—). When 10 wt% SN (SN:EO = 1:12) was added to a PEO-based solid-state electrolyte, as shown in Figure 1b, an inhomogeneous solid-state polymer electrolyte (Inhomo-SPE) was produced, within which an inhomogeneous phase and discontinuous Li^+ channels were formed, severely limiting the Li^+ transport. To construct a homogenous solid-state polymer electrolyte (Homo-SPE) with speculative continuous and fast Li^+ transport channels, more SN were required to form a mixed homogeneous phase with improved area (Figure 1c). This mixed homogeneous phase refers to a continuous composite architecture of PEO and SN on the scale of Li^+ binding sites, which produces continuous fast Li^+ transport channels in the electrolyte.

Free-standing films, named PEO32, Inhomo-SPE, and Homo-SPE, were prepared by solution casting (Figures 1d–f). Thermogravimetric analysis (TGA) suggested that the SN content are 10 wt% and 27 wt% in Inhomo-SPE and Homo-SPE, respectively (Figure S2, Supporting Information). Their surface morphologies were characterized by scanning electron microscope (SEM), as shown in Figures S3a–c, Supporting Information, in which the Homo-SPE exhibited a smoother and denser surface. The solution casting is a convenient method to prepare large-size membranes (Figure S3d, Supporting Information). This as-prepared Homo-SPE showed a characteristic peak of the —CN group at 2250 cm^{-1} in its FTIR spectrum, but not in PEO32. It also proved that there was no residual acetonitrile (also contains -CN) in the PEO-based electrolytes prepared by this method (Figure S4, Supporting Information).[33]

To understand the effect of SN content on the formation of speculative homogeneous electrolyte with fast ion transport channels, electrochemical impedance spectroscopy (EIS) measurements were carried out with calculating the corresponding ionic conductivities of various all-solid-state electrolytes. A molar ratio of Li^+: EO = 1:32 was chosen as the concentration of lithium salts. As shown in **Figure 2**a and Figure S5, Supporting Information, compared to typical PEO32, the ionic conductivity of the PEO-based electrolytes increased 10 times and 100 times (0.19 mS cm^{-1}) when a SN content reached SN:EO = 1:12 (≈10 wt% SN) and 1:4 (≈27 wt% SN), respectively. To verify that a high SN/EO ratio is favorable to improve the ionic conductivity, a lower concentration of lithium salt (Li^+: EO = 1:40) was chosen (Figures S6 and S7, Supporting Information). Even though with such a low Li^+ concentration, the PEO-based electrolyte still kept a high ionic conductivity of 0.28 mS cm^{-1} when the SN content of SN:EO = 1:4 was added. Overall, the PEO-based electrolytes with a higher SN/EO ratio have a higher ionic conductivity, because of the formation of homogeneous electrolytes with fast Li^+ transport channels.

To investigate the effect of SN on the crystallization behavior of Homo-SPE, differential scanning calorimetry (DSC) was used to study thermal transition of Homo-SPE and PEO32. As shown in Figure 2b, a typical peak associated with PEO32 at its melting temperature (T_m) of 60 °C is observed, the T_m of the resultant Homo-SPE reduced to 30 °C when 27 wt% SN was added. In addition, from the DSC curves recorded from 100 to 0 °C, the crystallization temperature (T_c) was about 30 °C for PEO32, but for the Homo-SPE no crystallization was

observed. Therefore, this fact suggests that adding SN into the PEO reduces its melting point and prevents its crystallization. Consequently, the absence of crystallization in the Homo-SPE results in the improvement of its ionic conductivity.[34,35] In addition, the crystallization behavior of Homo-SPE and PEO32 were investigated by X-ray diffraction (XRD) (Figure S8, Supporting Information). The calculated crystallinity is 89% for PEO32 and 29% for Homo-SPE. These results indicate that SN effectively inhibits the crystallization of PEO, which is beneficial to Li^+ transport.

To further explore the electrochemical performance of PEO-based electrolytes with channels for fast Li^+ transport, EIS measurements of different solid-state electrolytes were made at different working temperatures (Figure S9, Supporting Information). Figure 2c shows that the Homo-SPE has the highest ionic conductivity from 0–70 °C. The increased ionic conductivity of Homo-SPE with a high content of SN is attributed to two points. First, SN inhibits the crystallization of PEO and enhances the movement of PEO chains. Second but more importantly, a high SN/EO ratio in a PEO-based solid-state electrolyte is conducive to form the homogeneous electrolyte with fast Li^+ transport channels. In addition, time-dependent EIS measurements of the Homo-SPE were conducted at room temperature. The stable ionic conductivity with negligible increase was obtained over 3 months (Figure 2d; Figure S10, Supporting Information). This result shows that the Homo-SPE has considerable stability in ionic conductivity, which is favorable for all-solid-state batteries with long cycle life. Linear sweep voltammetry (LSV) measurement was also performed to measure a stable electrochemical window of the Homo-SPE (Figure S11, Supporting Information). It was found that the material has an oxidative stability of 4.7 V (vs. Li/Li^+), demonstrating it potentially useful in high-voltage cathode materials.

To evaluate the cycling stability of Homo-SPE, symmetric cells with lithium foils as both electrodes were assembled. As shown in Figure 2e, stripping and plating of the Homo-SPE was measured with 0.1 mAh cm^{-2} (0.1 mA cm^{-2}) at room temperature, and stable stripping and plating for at least 450 h without internal short-circuiting was observed. In contrast, in a Li|PEO32|Li cell it was relatively difficult to achieve the lithium deposition (inset in Figure 2e, black line) under a same condition, and a Li|Inhomo-SPE|Li cell exhibited poor cycling stability with a severely increased hysteresis potential. In addition, the Li^+ transference number (t_+) for the Homo-SPE was measured to be 0.48 (Figure S12, Supporting Information), much higher than that of PEO32 (t_+ = 0.16) (Figure S13, Supporting Information).

A series of electrochemical measurements were carried out to evaluate the electrochemical performance of Homo-SPE. **Figure 3**a shows the voltage profiles of various electrolytes (Liquid electrolyte (1 M $LiPF_6$ in EC/DEC), PEO32, Inhomo-SPE and Homo-SPE) within the voltage range 2.5–4.2 V (vs. Li/Li^+) at a current density of 0.5C (≈100 µA cm^{-2}). Compared with a Li|Liquid electrolyte|$LiFePO_4$ cell, an all-solid-state Li|Homo-SPE|$LiFePO_4$ cell has a slightly larger overpotential, but with a similar discharge capacity and a higher Coulombic efficiency at room temperature. However, Li|PEO32|$LiFePO_4$ and Li|Inhomo-SPE|$LiFePO_4$ cells have low discharge capacities under the same test conditions because of their poor ion conduction. As shown in Figure 3b, for the galvanostatic cycling performance of the Li|Homo-SPE|$LiFePO_4$ cell at 0.5 C, the highest discharge capacity reached 145.5 mAh g^{-1} at room temperature

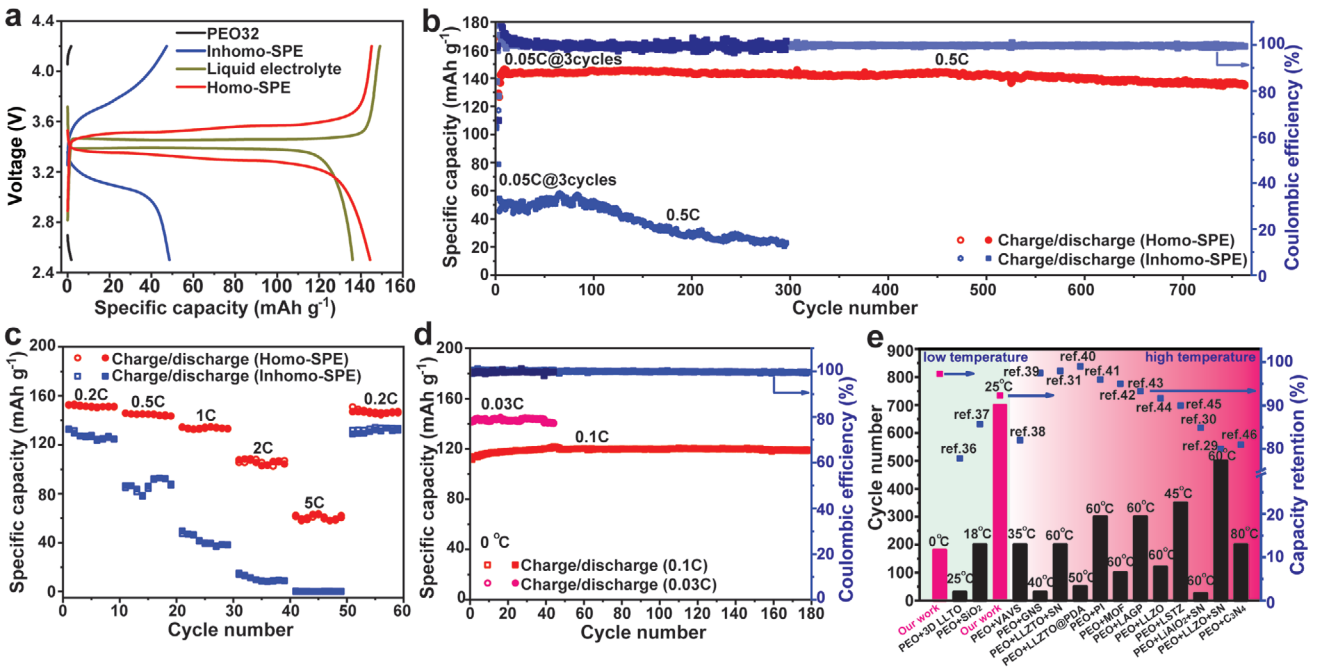

Figure 3. Full cell performance. a) Charge/discharge profiles of various electrolytes. b) Galvanostatic cycling performances of Li|Homo-SPE|$LiFePO_4$ and Li|Inhomo-SPE|$LiFePO_4$ cells at 0.5 C (25 °C). c) Rate capability of Li|Homo-SPE|$LiFePO_4$ and Li|Inhomo-SPE|$LiFePO_4$ cells at 25 °C. d) Galvanostatic cycling performances of Li|Homo-SPE|$LiFePO_4$ cells at 0 °C. e) The cycling performance of various PEO-based electrolytes plotted against capacity retention. Further details are included in Table S3, Supporting Information.

and this capacity maintained 135.7 mAh g^{-1} after 750 cycles. The Li|Inhomo-SPE|$LiFePO_4$ cell showed a low capacity (≈50 mAh g^{-1}) and poor cycling performance at 0.5 C, while the Li|PEO32|$LiFePO_4$ cell was even unable to charge and discharge at room temperature (Figure S14, Supporting Information). In addition, the rate capabilities were summarized in Figure 3c and Figure S15, Supporting Information. The Li|Homo-SPE|$LiFePO_4$ cell delivered a discharge capacity of 152.8, 145.3, 134.3, 105.7 and 61.5 mAh g^{-1} at 0.2 C, 0.5 C, 1 C, 2 C and 5 C, respectively. In contrast, the Li|Inhomo-SPE|$LiFePO_4$ cell had a much lower discharge capacity and worse stability. Even at 1 C, the Homo-SPE enabled the $LiFePO_4$ cathode to achieve a stable cycling performance with a discharge capacity of 100 mAh g^{-1} after 1200 cycles (Figure S16, Supporting Information). Decreasing the adding amount of lithium salt in PEO-based solid-state electrolytes effectively improves its mechanical properties (Figure S17, Supporting Information). PEO-based membrane with a lower Li^+ concentration (Li^+: EO = 1:40) was also used as an all-solid-state electrolyte (Homo-SPE-2), and its corresponding Li|Homo-SPE-2|$LiFePO_4$ cell had a high discharge capacity (121.3 mAh g^{-1}) and long cycling stability (≈350 cycles) at room temperature (Figure S18, Supporting Information). To verify that the molar ratio of SN:EO = 1:4 is enough to construct homogeneous and fast Li^+ transport channels. We have tried to increase the SN content to SN:EO = 1:1, however, the addition of such a large number of SN would decrease its mechanical properties, which makes it difficult to form free-standing films. To form a free-standing film with SN:EO = 1:1, the LiTFSI content was adjusted to Li^+: EO = 1:80. As a result, compared with Homo-SPE, free-standing PEO-based electrolyte with higher SN content (SN:EO = 1:1) and lower Li^+ concentration (Li^+:EO = 1:80) showed poor rate performance at room temperature (Figure S19, Supporting Information).

Due to the homogeneous and fast Li^+ transport channels of Homo-SPE, Li|Homo-SPE|$LiFePO_4$ cell exhibited excellent electrochemical performance at 15 °C, As shown in Figure S20a, Supporting Information, the Li|Homo-SPE|$LiFePO_4$ cell delivered a discharge capacity of 146.2, 135.5, 100.6 and 49.1 mAh g^{-1} at 0.1 C, 0.2 C, 0.5 C and 1 C, respectively. And for the galvanostatic cycling performance of the Li|Homo-SPE|$LiFePO_4$ cell at 0.2 C, discharge capacity maintained 130.3 mAh g^{-1} after 44 cycles (Figure S20b, Supporting Information). It was also found that the Li|Homo-SPE|$LiFePO_4$ cell had a high capacity even at 0 °C. As shown in Figure 3d and Figure S21, Supporting Information, the stable cycling performance could be obtained with a discharge capacity of 118.6 mAh g^{-1} after 180 cycles at 0.1 C, and a high capacity of 141.5 mAh g^{-1} at 0.03 C. It is the first time to fabricate a Li|PEO-based electrolyte|$LiFePO_4$ cell with a high capacity and long cycling life at 0 °C. Moreover, Homo-SPE is also suitable for high-voltage cathode materials. The corresponding results for a Li|Homo-SPE|NCM811 cell are shown in Figure S22, Supporting Information, which shows a high Coulombic efficiency and high cycling stability at room temperature. Furthermore, in order to measure the stability of Homo-SPE in air, a Li|Homo-SPE|$LiFePO_4$ cell was assembled with Homo-SPE which had been kept in the air for 24 h. As shown in Figure S23, Supporting Information, its electrochemical performance had not changed significantly. This result indicates that Homo-SPEs are not sensitive to moisture and air.

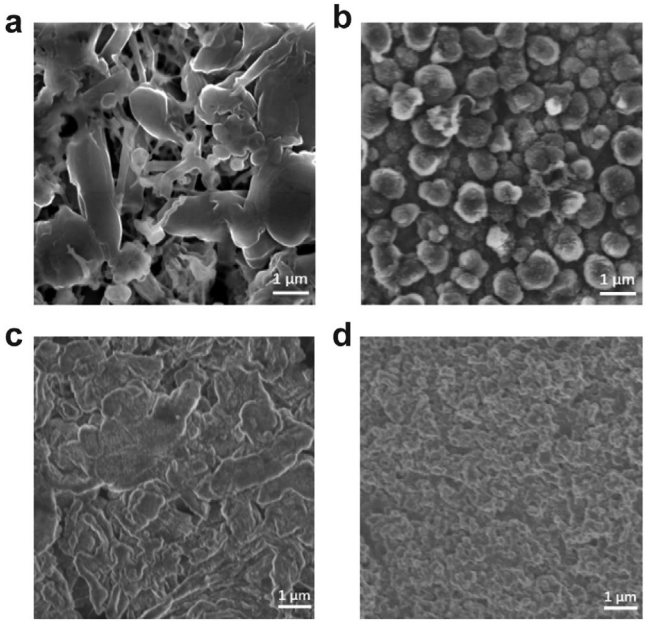

Figure 4. Characterization of lithium deposition morphology. SEM images of lithium electrodeposition on Cu with a) a liquid electrolyte (1M $LiPF_6$ in EC/DEC) and b) Homo-SPE at 0.1 mAh cm^{-2}. SEM images of a lithium anode in Li|electrolytes|$LiFePO_4$ cells with c) a liquid electrolyte (1 M $LiPF_6$ in EC/DEC) and d) Homo-SPE.

Figure 3e summarizes the cycling performance and capacity retention of different PEO-based electrolytes for Li|PEO-based electrolyte|$LiFePO_4$ cells reported in the literature during the last two years (Table S3, Supporting Information).[29–31,36–46] Compared to other methods, our PEO-based electrolytes are a simple and low-cost way to make cells that work at both room temperature and lower temperature of 0 °C. Our Li|Homo-SPE|$LiFePO_4$ cell presented good cycling performance (≈750 cycles) and high capacity retention (92.3%) at room temperature. And even at 0 °C, it still delivered good cycling performance (≈180 cycles) and high capacity retention (97.3%).

SEM was used to investigate the effect of Homo-SPE on the lithium deposition. **Figure 4**a and 4b show the lithium deposition morphology on Cu from disassembled Li|1M $LiPF_6$ EC-DEC|Cu and Li|Homo-SPE|Cu cells after cycling. It is clear that lithium deposited unevenly and dendrites were formed when a liquid electrolyte was used (Figure 4a). For the Homo-SPE, however, the morphology of the lithium deposition was rather uniform without lithium dendrites (Figure 4b). The surface of lithium metal from a disassembled Li|1M $LiPF_6$ EC/DEC|$LiFePO_4$ cell after 200 cycles was uneven (Figure 4c). Even when the cycling number is twice that of the cell with liquid electrolyte, the morphology of a lithium metal anode from a disassembled Li|Homo-SPE|$LiFePO_4$ cell after 400 cycles was very uniform due to the protection of Homo-SPE (Figure 4d). This is because, different with liquid electrolytes, PEO has a low exchange current density and high surface energy, which promotes the growth of small Li particles and the increase of lithium nucleation density, leading to more uniform lithium deposition.[47] Moreover, SN-based interlayer was also reported to prevent the lithium dendrite formation due to the formation of a passivation layer on the Li metal surface.[48]

Therefore, Homo-SPE as an electrolyte for all-solid-state cell is beneficial for uniform lithium deposition. The chemical compositions of the SEI layer formed on the lithium anode after cycling were further analyzed by X-ray photoelectron spectroscopy (XPS), as shown in Figure S24, Supporting Information, the SEI layer of Homo-SPE with an abundance of Li_3N and LiF, which contributes to the uniform deposition morphology and long cycle stability.

To understand the Li^+ transport mechanism in Homo-SPE, the solid-state nuclear magnetic resonance (NMR) experiments were performed. ^7Li solid-state NMR spectra are shown in **Figure 5**a, the changes of Li^+ chemical environment reflect the interaction between SN/PEO and Li^+. Compared with the PEO32 (PEO+LiTFSI), the ^7Li NMR signals of Homo-SPE shifted 0.50 ppm upfield, the shifting up-field of Li resonance in Homo-SPE implies a weakened PEO-Li^+ interaction.[49,50] Thus, the addition of SN can mitigate the affinity between EO and Li^+. Figure 5b shows the ^1H solid-state NMR spectra of SN+LiTFSI, PEO32 and Homo-SPE. The ^1H NMR signal at 2.8 ppm is assigned to hydrogen in SN (NC–CH_2–CH_2–CN) and the signal at around 3.5–4.0 ppm is attributed to hydrogen in PEO (–O–CH_2–CH_2–O–). There are two configurations of PEO32 in complexation with Li^+, *trans*-PEO (where adjacent O atoms are in the *para*-position) and *cis*-PEO (where adjacent O atoms are in the *ortho*-position), which leads to two ^1H signals at 3.56 and 3.88 ppm, respectively. When SN was added into PEO, the *cis*-PEO at 3.88 ppm disappears and only *trans*-PEO at 3.56 ppm remains, due to the weakened interaction between

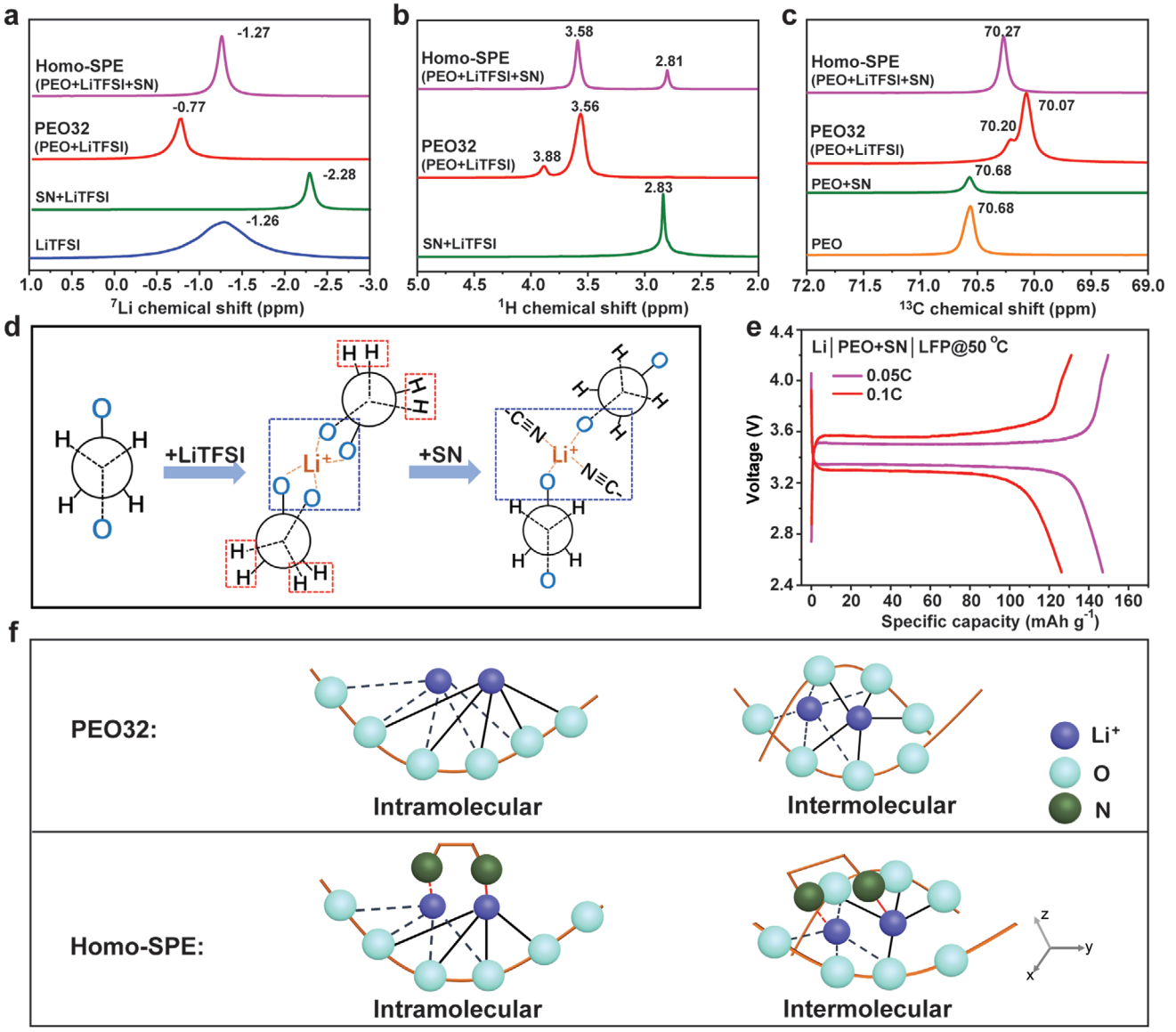

Figure 5. Li^+ transport mechanism in Homo-SPE. a) ^7Li solid-state NMR spectra of LiTFSI, SN+LiTFSI, PEO32, and Homo-SPE. b) ^1H solid-state NMR spectra of SN+LiTFSI, PEO32, and Homo-SPE. c) ^{13}C NMR spectra of PEO, PEO+SN, PEO32, and Homo-SPE measured in $CDCl_3$. d) Carbon conformation transition diagram of PEO, PEO32, and Homo-SPE. e) Charge/discharge profiles of Li|PEO+SN|$LiFePO_4$ cell at 50 °C. f) Li^+ transport mechanism in PEO32 and Homo-SPE.

Li^+ and PEO. Importantly, ^7Li and ^1H solid-state NMR measurements of Homo-SPE were also carried out after 100 cycles, there is no clear change of ^7Li and ^1H chemical shift of the cycled Homo-SPE (Figure S25, Supporting Information), which means a stable Li^+ chemical environment and stable structure of PEO and SN in Homo-SPE during charge and discharge.

In order to elucidate the effect of Li^+ and SN on the conformation of PEO, ^{13}C NMR experiments was also conducted to probe the difference of chemical environment of carbon in PEO, SN, PEO+LiTFSI, PEO+SN and Homo-SPE (Figure S26, Supporting Information). The ^{13}C signal at around 70 ppm is attributed to carbon in PEO (–CH_2–O–), and the signals at around 14 and 116 ppm are attributed to methylene and nitride groups of SN, respectively.[51] As shown in Figure 5c, there is only one ^{13}C signal at 70.68 ppm observed for PEO and PEO+SN membranes, which is consistent with the *trans*-PEO as shown in Figure S27a, Supporting Information. However, as LiTFSI was added into PEO, two signals at 70.07 and 70.20 ppm formed were observed, which are attributed to *cis*-PEO and *trans*-PEO, respectively, in complexation with Li^+ (Figure S27b, Supporting Information). When SN was added into PEO+LiTFSI complex, the strong interaction between SN and Li^+ results in only one observed ^{13}C signal (*trans*-PEO) in Homo-SPE, which is consistent with ^1H NMR results. The relevant carbon conformation diagram was shown in Figure S27c, Supporting Information. Therefore, based on ^7Li, ^1H and ^{13}C NMR spectra, the possible conformation transition diagram of PEO are shown in Figure 5d, which clearly reveal the effect of Li^+ and SN on PEO conformation.

To clearly show that the size of SN matches the distance between the adjacent Li^+ binding sites in the PEO, organic molecular materials with different lengths were chosen as fillers (Succinonitrile, Adiponitrile and Sebaconitrile). Figure S28, Supporting Information, shows the Li^+ transport process and related electrochemical properties determined by the size of the fillers, and the galvanostatic cycling performances indicate that PEO-based composite electrolytes could perform better performance when the size of fillers (SN) matches the length of –O–CH_2–CH_2–O–. Considering the fast transport of Li^+ in PEO-based solid-state electrolytes may not depend on the existence of lithium salt, a PEO+SN membrane (SN:EO = 1:4) without any lithium salt was also prepared to verify the positive effect of homogeneous electrolyte with fast Li^+ transport channels formed in PEO+SN systems (Figure S29, Supporting Information). Chronoamperometry (CA) and EIS of the PEO+SN membrane before and after CA are shown in Figures S30 and S31, Supporting Information. The PEO+SN membrane displayed a Li^+ transference number as high as 0.7, although its ionic conductivity is 0.0025 mS cm^{-1} at 50 °C. The Li|PEO+SN|$LiFePO_4$ cell showed good capacities of 126.2 mAh g^{-1} and 146.9 mAh g^{-1} at 0.1 C and 0.05 C (Figure 5e). However, Li^+ transport in pure PEO and SN membranes was difficult under the same conditions (Figure S32, Supporting Information), which proves that fast ion transport channels within homogeneous electrolytes are constructed in the PEO+SN membrane. Although fast Li^+ channels can be formed into PEO+SN systems without lithium salt, the lithium salt is necessary for these systems, otherwise, PEO+SN membranes exhibits low ionic conductivity and poor cycling stability (Figure S33, Supporting Information). A possible Li^+ transport mechanism in Homo-SPE is then proposed and is shown in Figure 5f. The added SN weakens the affinity between EO and Li^+ and contributes to the formation of continuous and fast Li^+ transport channels in the homogenous PEO-based electrolyte.

3. Conclusion

We demonstrate a simple but effective method to improve the low temperature electrochemical performance of PEO-based solid-state electrolytes by constructing fast ion transport channels. Homo-SPE with fast Li^+ transport channels was formed by adding a high content of SN, and meanwhile, a low content of lithium salt was applied to tackle the challenge that a free-standing membrane is difficult to form with a high SN content. All-solid-state lithium cells were then fabricated based on these Homo-SPE, which showed an excellent cycling performance at room temperature and a lower temperature of 0 °C. A high SN/EO ratio was found to inhibit the crystallization of PEO and to form a homogeneous PEO-based solid-state electrolyte with fast Li^+ transport channels. This design opens up a new pathway to prepare all-solid-state lithium batteries that can be used at room temperature or lower.

4. Experimental Section

Preparation of PEO-Based Solid-State Electrolytes: The PEO-based solid-state electrolytes were prepared by a solution casting method. For convenience, the thickness of the solid-state electrolyte was kept at about 150 µm. To form PEO32, 1.00 g PEO and 0.203 g LiTFSI (Li^+: EO = 1:32) were dissolved in acetonitrile and a homogeneous solution was formed by stirring for 24 h at room temperature. The slurry was then cast onto a horizontal Teflon plate and dried in a vacuum oven at 40 °C for 24h to remove most of the acetonitrile solvent, and continued to vacuum dry at 50 °C for 48 h to completely evaporate acetonitrile solvent. For Inhomo-SPE, 1.00 g PEO and 0.356 g LiTFSI (Li^+: EO = 1:18) were dissolved in acetonitrile and homogeneous solution was formed after stirring for 24 h at room temperature. 0.150 g SN was then added to the above homogeneous solution and stirred for 12 h. The forming and drying procedures were identical to that use for PEO32. For the Homo-SPE, 1.00 g PEO and 0.203 g LiTFSI (Li^+: EO = 1:32) were dissolved in acetonitrile and homogeneous solution was formed after stirring for 24 h at room temperature. 0.450 g SN was then added to the above homogeneous solution and stirred for 12 h. The forming and drying procedures were identical to that use for PEO32. For Homo-SPE-2, 1.00 g PEO and 0.158 g LiTFSI (Li^+: EO = 1:40) were dissolved in acetonitrile and homogeneous solution was formed after stirring for 24 h at room temperature. 0.450 g SN was added to the above homogeneous solution and stirred for 12 h. The slurry was cast onto a horizontal Teflon plate and dried in a vacuum oven at 40 °C for 24h to remove most of the acetonitrile solvent, and continued to vacuum dry at 50 °C for 48 h to completely evaporate acetonitrile solvent. For PEO+SN, 1.00 g PEO were dissolved in acetonitrile and homogeneous solution was formed after stirring for 24 h at room temperature. 0.450 g SN was added to the above homogeneous solution and stirred for 12 h. The slurry was cast onto a horizontal Teflon plate and dried in a vacuum oven at 40 °C for 24h to remove most of the acetonitrile solvent, and continued to vacuum dry at 50 °C for 48 h to completely evaporate acetonitrile solvent.

Preparation of Cathodes: 60 wt% LFP or NCM811, 15 wt% Super-P, 15 wt% PVDF (polyvinylidene fluoride) and 10 wt% Homo-SPE were mixed together with *N*-methyl pyrrolidinone (NMP) to form a uniform slurry that was coated on aluminum foils and dried in a vacuum oven at 80 °C for 24 h. The foils were cut into circular cathodes with a diameter of 12 mm. The loading of LFP or NCM811 was around 1.0 mg cm^{-2}.

Cell Assembly and Measurements: In this study, all electrochemical tests were carried out using CR2025-type coin cells. The cells structure was shown in Figure S34, Supporting Information, first, the cathode is placed in the positive shell, second, the solid-state electrolyte membrane and the lithium anode are placed in turn, then the nickel foam is added and the negative shell is finally covered. All of the cells were fabricated in an Ar-filled glove box (O_2 < 0.1 ppm, H_2O < 0.1 ppm). For liquid electrolyte cells, Celgard 2400 and 1M $LiPF_6$ in EC/DEC were used to replace the all-solid-state electrolyte. A Landian multichannel battery tester was used to perform electrochemical measurements. The charge-discharge voltage range was 2.5–4.2 V for LFP cathodes and 3.0–4.3 V for NCM811 cathodes. The 1 C rate is determined to be 170 and 275 mA g^{-1} in LFP and NCM811 cell testing respectively.

Electrochemical Measurements: Electrochemical measurements were carried out on an electrochemical station (Biologic VSP-300). The ionic conductivity of the solid-state electrolytes was measured by electrochemical impedance spectroscopy (EIS) with a frequency range from 0.1 Hz to 3M Hz and an amplitude voltage of 10 mV. A corresponding cell was assembled using two polished stainless-steel blocking electrodes in a glove box under an argon atmosphere. Before testing, all cells were placed in an incubator (50 °C) for 4h and then allowed to stand at room temperature for 12 h. The ionic conductivity σ was calculated from the following equation:

$$\sigma = \frac{d}{S \times R_b} \tag{1}$$

where d (cm) is the thickness of the solid-state membrane, S (cm^2) is the area of the stainless-steel electrode, and R_b (Ω) is the bulk resistance of the electrolyte membrane measured by EIS. The electrochemical stability window of the solid-state electrolytes was obtained at room temperature by linear sweep voltammetry (LSV) using stainless-steel as the working electrode and a lithium metal as the counter electrode at a scan rate of 0.5 mV s^{-1} from 2.0 to 6.0 V. The Li^+ transference number (t_+) of the solid-state electrolyte was measured by a chronoamperometry test on a Li|electrolyte|Li cell with an applied voltage of 10 mV. On the basis of the measured values, t_+ was calculated by following equation:

$$t_+ = \frac{I_s(\Delta V - I_0 R_0)}{I_0(\Delta V - I_s R_s)} \tag{2}$$

where ΔV (V) is the potential applied across the cell, and the initial (I_0) and steady-state (I_s) currents are obtained from the chronoamperometric curve. R_0 and R_s measured by EIS reflect the initial and steady-state resistances of the passivating layers.

Materials Characterizations: X-ray diffraction (XRD) patterns were recorded on a Rigaku diffractometer using Cu Kα radiation at room temperature. ATR-FTIR spectra were recorded on a Nicolet iS5 iD7 ATR spectrometer equipped with a diamond KBr beam splitter and an empty ATR cell blanketed with argon was used to collect the background spectrum. The morphology of the samples was characterized using a scanning electron microscope (SEM, FEI Nova Nano SEM 430, 10 kV). TGA was performed with a NETZSCH STA 449 C thermo balance in argon with a heating rate of 10 °C min^{-1} from room temperature to 800 °C. Differential scanning calorimetry of the electrolyte materials was recorded on a DSC214 (NETZSCH) from 0 to 100 °C and 100 to 0 °C. ^1H and ^7Li solid-state MAS NMR experiments were performed on a Bruker AVANCE III 400 MHz NMR spectrometer using a 4mm DVT MAS NMR probe, with ^1H and ^7Li Larmor frequencies of 400.2 and 155.5 MHz, respectively, and the samples were packed into the center of the rotors and the spinning rates were set to 8≈10 kHz. ^{13}C NMR experiments were performed using a Bruker AVANCE III 600 of 150.9 MHz, and $CDCl_3$ (containing 0.03% V/V TMS) as solvent at room temperature.

Supporting Information

Supporting Information is available from the Wiley Online Library or from the author.

Acknowledgements

S.X. and Z.S. contributed equally to this work. The authors acknowledge financial support from National Natural Science Foundation of China (Nos. 51972313, 51927803, 51525206), National Key R&D Program of China (2016YFA0200102 and 2016YFB0100100), the Strategic Priority Research Program of the Chinese Academy of Sciences (XDA22010602), Youth Innovation Promotion Association of the Chinese Academy of Sciences (No. Y201942), the Special Projects of the Central Government in Guidance of Local Science and Technology Development (No. 2020JH6/10500024), the Key Research Program of the Chinese Academy of Sciences (Grant No. KGZD-EW-T06). The Bureau of Industry and Information Technology of Shenzhen for the "2017 Graphene Manufacturing Innovation Center Project" (No. 201901171523).

Conflict of Interest

The authors declare no conflict of interest.

Keywords

homogeneous ion conduction, lithium batteries, poly ethylene oxide, solid-state electrolytes

Received: August 24, 2020
Published online:

[1] M. Armand, J. M. Tarascon, *Nature* **2008**, *451*, 652.
[2] R. Chen, Q. Li, X. Yu, L. Chen, H. Li, *Chem. Rev.* **2020**, *120*, 6820.
[3] A. Manthiram, X. Yu, S. Wang, *Nat. Rev. Mater.* **2017**, *2*, 16103.
[4] D. Zhou, D. Shanmukaraj, A. Tkacheva, M. Armand, G. Wang, *Chem* **2019**, *5*, 2326.
[5] X. Yang, Q. Sun, C. Zhao, X. Gao, K. Adair, Y. Zhao, J. Luo, X. Lin, J. Liang, H. Huang, L. Zhang, S. Lu, R. Li, X. Sun, *Energy Storage Mater.* **2019**, *22*, 194.
[6] K. Pan, L. Zhang, W. Qian, X. Wu, K. Dong, H. Zhang, S. Zhang, *Adv. Mater.* **2020**, *32*, 2000399.
[7] H. Zhang, C. Li, M. Piszcz, E. Coya, T. Rojo, L. M. Rodriguez-Martinez, M. Armand, Z. Zhou, *Chem. Soc. Rev.* **2017**, *46*, 797.
[8] K. K. Fu, Y. Gong, J. Dai, A. Gong, X. Han, Y. Yao, C. Wang, Y. Wang, Y. Chen, C. Yan, Y. Li, E. D. Wachsman, L. Hu, *Proc. Natl. Acad. Sci. U. S. A.* **2016**, *113*, 7094.
[9] I. Osada, H. de Vries, B. Scrosati, S. Passerini, *Angew. Chem., Int. Ed.* **2016**, *55*, 500.
[10] E. D. Gomez, A. Panday, E. H. Feng, V. Chen, G. M. Stone, A. M. Minor, C. Kisielowski, K. H. Downing, O. Borodin, G. D. Smith, N. P. Balsara, *Nano Lett.* **2009**, *9*, 1212.
[11] Z. Xue, D. He, X. Xie, *J. Mater. Chem. A* **2015**, *3*, 19218.
[12] F. Croce, G. B. Appetecchi, L. Persi, B. Scrosati, *Nature* **1998**, *394*, 456.
[13] A. Manuel Stephan, K. S. Nahm, *Polymer* **2006**, *47*, 5952.
[14] W. Liu, S. W. Lee, D. Lin, F. Shi, S. Wang, A. D. Sendek, Y. Cui, *Nat. Energy* **2017**, *2*, 17035.
[15] J. Bae, Y. Li, J. Zhang, X. Zhou, F. Zhao, Y. Shi, J. B. Goodenough, G. Yu, *Angew. Chem., Int. Ed.* **2018**, *57*, 2096.
[16] Y. Zhang, R. Chen, S. Wang, T. Liu, B. Xu, X. Zhang, X. Wang, Y. Shen, Y.-H. Lin, M. Li, L.-Z. Fan, L. Li, C.-W. Nan, *Energy Storage Mater.* **2020**, *25*, 145.
[17] N. Wu, P. H. Chien, Y. Qian, Y. Li, H. Xu, N. S. Grundish, B. Xu, H. Jin, Y. Y. Hu, G. Yu, J. B. Goodenough, *Angew. Chem., Int. Ed.* **2020**, *59*, 4131.

[18] T. F. Miller3rd, Z. G. Wang, G. W. Coates, N. P. Balsara, *Acc. Chem. Res.* **2017**, *50*, 590.
[19] M. Li, C. Wang, Z. Chen, K. Xu, J. Lu, *Chem. Rev.* **2020**, *120*, 6783.
[20] P. G. Bruce, C. A. Vincent, *J. Chem. Soc., Faraday Trans.* **1993**, *89*, 3187.
[21] Z. Stoeva, I. Martin-Litas, E. Staunton, Y. G. Andreev, P. G. Bruce, *J. Am. Chem. Soc.* **2003**, *125*, 4619.
[22] P. Johansson, J. Tegenfeldt, J. lindgren, *Polymer* **2001**, *42*, 6573.
[23] H. Abroshan, N. R. Dhumal, Y. Shim, H. J. Kim, *Phys. Chem. Chem. Phys.* **2016**, *18*, 6754.
[24] P. J. Alarco, Y. Abu-Lebdeh, A. Abouimrane, M. Armand, *Nat. Mater.* **2004**, *3*, 476.
[25] Y. Ugata, M. L. Thomas, T. Mandai, K. Ueno, K. Dokko, M. Watanabe, *Phys. Chem. Chem. Phys.* **2019**, *21*, 9759.
[26] L. Z. Fan, Y. S. Hu, A. J. Bhattacharyya, J. Maier, *Adv. Funct. Mater.* **2007**, *17*, 2800.
[27] M. Echeverri, N. Kim, T. Kyu, *Macromolecules* **2012**, *45*, 6068.
[28] Y.-C. Jung, M.-S. Park, C.-H. Doh, D.-W. Kim, *Electrochim. Acta* **2016**, *218*, 271.
[29] F. Chen, W. Zha, D. Yang, S. Cao, Q. Shen, L. Zhang, D. R. Sadoway, *J. Electrochem. Soc.* **2018**, *165*, A3558.
[30] N. Zhang, J. He, W. Han, Y. Wang, *J. Mater. Sci.* **2019**, *54*, 9603.
[31] W. Zha, F. Chen, D. Yang, Q. Shen, L. Zhang, *J. Power Sources* **2018**, *397*, 87.
[32] B. Chen, Z. Huang, X. Chen, Y. Zhao, Q. Xu, P. Long, S. Chen, X. Xu, *Electrochim. Acta* **2016**, *210*, 905.
[33] D. Zhou, Y.-B. He, R. Liu, M. Liu, H. Du, B. Li, Q. Cai, Q.-H. Yang, F. Kang, *Adv. Energy Mater.* **2015**, *5*, 1500353.
[34] X. Zhang, J. Xie, F. Shi, D. Lin, Y. Liu, W. Liu, A. Pei, Y. Gong, H. Wang, K. Liu, Y. Xiang, Y. Cui, *Nano Lett.* **2018**, *18*, 3829.
[35] Q. Zhao, X. Liu, S. Stalin, K. Khan, L. A. Archer, *Nat. Energy* **2019**, *4*, 365.
[36] X. Wang, Y. Zhang, X. Zhang, T. Liu, Y. H. Lin, L. Li, Y. Shen, C. W. Nan, *ACS Appl. Mater. Interfaces* **2018**, *10*, 24791.
[37] D. Lin, P. Y. Yuen, Y. Liu, W. Liu, N. Liu, R. H. Dauskardt, Y. Cui, *Adv. Mater.* **2018**, *30*, 1802661.
[38] W. Tang, S. Tang, X. Guan, X. Zhang, Q. Xiang, J. Luo, *Adv. Funct. Mater.* **2019**, *29*, 1900648.
[39] S. Song, Y. Wu, W. Tang, F. Deng, J. Yao, Z. Liu, R. Hu, Alamusi, Z. Wen, L. Lu, N. Hu, *ACS Sustainable Chem. Eng.* **2019**, *7*, 7163.
[40] Z. Huang, W. Pang, P. Liang, Z. Jin, N. Grundish, Y. Li, C.-A. Wang, *J. Mater. Chem. A* **2019**, *7*, 16425.
[41] J. Wan, J. Xie, X. Kong, Z. Liu, K. Liu, F. Shi, A. Pei, H. Chen, W. Chen, J. Chen, X. Zhang, L. Zong, J. Wang, L. Q. Chen, J. Qin, Y. Cui, *Nat. Nanotechnol.* **2019**, *14*, 705.
[42] J.-F. Wu, X. Guo, *J. Mater. Chem. A* **2019**, *7*, 2653.
[43] X. Wang, H. Zhai, B. Qie, Q. Cheng, A. Li, J. Borovilas, B. Xu, C. Shi, T. Jin, X. Liao, Y. Li, X. He, S. Du, Y. Fu, M. Dontigny, K. Zaghib, Y. Yang, *Nano Energy* **2019**, *60*, 205.
[44] Z. Wan, D. Lei, W. Yang, C. Liu, K. Shi, X. Hao, L. Shen, W. Lv, B. Li, Q.-H. Yang, F. Kang, Y.-B. He, *Adv. Funct. Mater.* **2019**, *29*, 1805301.
[45] H. Xu, P. H. Chien, J. Shi, Y. Li, N. Wu, Y. Liu, Y. Y. Hu, J. B. Goodenough, *Proc. Natl. Acad. Sci. U. S. A.* **2019**, *116*, 18815.
[46] J. Yang, X. Wang, G. Zhang, A. Ma, W. Chen, L. Shao, C. Shen, K. Xie, *Front. Chem.* **2019**, *7*, 388.
[47] J. Lopez, A. Pei, J. Y. Oh, G. N. Wang, Y. Cui, Z. Bao, *J. Am. Chem. Soc.* **2018**, *140*, 11735.
[48] H. Zhang, X. Judez, A. Santiago, M. Martinez-Ibañez, M. Á. Muñoz-Márquez, J. Carrasco, C. Li, G. G. Eshetu, M. Armand, *Adv. Energy Mater.* **2019**, *9*, 1900763.
[49] N. Wu, P. H. Chien, Y. Li, A. Dolocan, H. Xu, B. Xu, N. S. Grundish, H. Jin, Y. Y. Hu, J. B. Goodenough, *J. Am. Chem. Soc.* **2020**, *142*, 2497.
[50] J. Zheng, H. Dang, X. Feng, P.-H. Chien, Y.-Y. Hu, *J. Mater. Chem. A* **2017**, *5*, 18457.
[51] N. Voigt, L. van Wüllen, *Solid State Ionics* **2014**, *260*, 65.